

Stochastic Mutation as a Mechanism for the Emergence of SARS-CoV-2 New Variants

Liaofu Luo ^{1,*} and Jun Lv ^{2,*}

ORCID: 0000-0002-6822-185X (Liaofu Luo); 0000-0002-4546-535X (Jun Lv)

¹Faculty of Physical Science and Technology, Inner Mongolia University, Hohhot 010021, China

²College of Science, Inner Mongolia University of Technology, Hohhot 010051, China

*Correspondence: Liaofu Luo, lolfcm@imu.edu.cn; Jun Lv, lujun@imut.edu.cn (point of communication)

Abstract

Predicting the future evolutionary trajectory of SARS-CoV-2 remains a critical challenge, particularly due to the pivotal role of spike protein mutations. It is therefore essential to develop evolutionary models capable of continuously integrating new experimental data. In this study, we employ a cladogram algorithm that incorporates established assumptions for mutant representation—using both four-letter and two-letter formats—along with an n -mer distance algorithm to construct a cladogenetic tree of SARS-CoV-2 mutations. This tree accurately captures the observed changes across macro-lineages. We introduce a stochastic method for generating new strains on this tree based on spike protein mutations. For a given set A of existing mutation sites, we define a set X comprising x randomly generated mutation sites on the spike protein. The intersection of A and X , denoted as set Y , contains y sites. Our analysis indicates that the position of a generated strain on the tree is primarily determined by x . Through large-scale stochastic sampling, we predict the emergence of new macro-lineages. As x increases, the dominance among macro-lineages shifts: lineage O surpasses N, P surpasses O, and eventually Q surpasses P. We identify threshold values of x that delineate transitions between these macro-lineages. Furthermore, we propose an algorithm for predicting the timeline of macro-lineage emergence. In conclusion, our findings demonstrate that SARS-CoV-2 evolution adheres to statistical principles: the emergence of new strains can be driven by randomly generated spike protein sites, and large-scale stochastic sampling reveals evolutionary patterns underlying the rise of distinct macro-lineages.

Keywords

SARS-CoV-2, spike protein mutation, evolutionary analysis

1 Introduction

Over the past five years, Severe Acute Respiratory Syndrome Coronavirus 2 (SARS-CoV-2) has undergone continuous mutation, giving rise to numerous variants such as Alpha, Beta, Gamma, Delta, and Omicron. The complex interplay among viral antigenicity, transmissibility, and

virulence complicates predictions regarding the future trajectory and disease burden of Coronavirus Disease 2019 (COVID-19) [1-6]. Recent studies have introduced innovative approaches for forecasting pandemic evolution. For example, a network-based inference method has been proposed for short- to medium-term predictions, though its reliability decreases for long-term forecasting [7]. Given the crucial role of spike protein mutations in SARS-CoV-2 evolution, deep learning techniques—particularly those utilizing Large Language Models—have been developed to predict future protein sequences [8-11]. Among these, the PandoGen algorithm has shown promise in training protein language models for pandemic-related protein forecasting [8]. However, challenges persist in applying PandoGen to predict recombinant SARS-CoV-2 lineages and in ensuring the continuous incorporation of new experimental data.

Recent literature has emphasized the influence of biological driving factors on mutational probability [12-16]. Viral evolution is primarily driven by two key factors: intrinsic transmissibility, determined by SARS-CoV-2's angiotensin-converting enzyme 2 (ACE2) binding affinity, and immune evasion. Studies have observed numerous immune-evasive mutations in Omicron subvariants, indicating that immune pressure correlates with the accumulation of immune escape mutations, with similar pressure patterns observed among variants within the same macro-lineage. Additionally, computational analyses of affinity dynamics have been explored. These findings collectively contribute to the refinement of our model.

Building upon the driving force of immune evasion and its relationship with affinity dynamics, we propose an evolutionary model for viral mutations. First, utilizing the 4-letter mutant representation and its relationship with the 2-letter representation, along with a robust tree construction algorithm, we construct an evolutionary tree that accurately reflects observed evolutionary patterns of existing viral strains. Subsequently, integrating the concept of stochastic immune escape mutation, we develop a statistical method termed the A-X model [17], extending the utility of the evolutionary tree to predict the emergence of novel macro-lineages.

Our findings indicate that the probability of macro-lineage emergence correlates with the number of stochastically mutated sites on the spike protein. As this number increases, macro-lineage proportions shift sequentially: lineage O surpasses N, followed by P surpassing O, and ultimately Q surpassing P. We successfully predicted the emergence of macro-lineage P, which has since been validated.

In a previous study [18], we developed a mathematical model to analyze COVID-19 transmission dynamics, particularly focusing on explaining the second wave of SARS-CoV-2 infections and investigating competitive transmission between two viral strains within a region. Crucially, predicting new macro-lineage emergence is closely linked to such competitive dynamics. These results provide a vital theoretical foundation for understanding SARS-CoV-2 evolution.

A further challenge involves accurately predicting the evolutionary timeline of SARS-CoV-2. To forecast the future trajectory of macro-lineage P and the potential emergence of a macro-lineage Q, it is essential to understand how the number of mutated sites on the spike protein of selected SARS-CoV-2 variants changes over time. Despite the complexity of factors influencing viral evolution, we observed an approximately linear relationship between the number of mutated sites in a given variant and the date of its first global sample collection. This

relationship enables the development of an algorithm to predict the timeline of macro-lineage transformations.

2 Methods

2.1 ACE2 binding affinity of single mutations and four-letter representation of mutants

We obtained data on single-point mutations affecting the interaction between the receptor-binding domain (RBD) – spanning amino acid residues 331 to 531 of the spike protein – and the ACE2 receptor from references [19, 20]. For each mutation at residue i , the mean and standard deviation of the binding affinity are denoted as b_i and s_i , respectively. A mutation is classified as affinity-enhancing if its measured affinity m_i satisfies $m_i > b_i + s_i$; affinity-weakening if $m_i < b_i - s_i$; and negligible in effect if $b_i - s_i \leq m_i \leq b_i + s_i$.

The surface of coronaviruses is decorated with a spike protein, which in SARS-CoV-2 consists of approximately 1273 amino acids. Each SARS-CoV-2 strain is represented by a four-letter sequence, where each letter indicates the mutation type at a specific residue. The encoding is defined as follows: 0 denotes no mutation relative to the wild type; 1 indicates a mutation with negligible effect on ACE2 binding affinity; 2 represents an affinity-enhancing mutation; and 3 signifies an affinity-weakening mutation. Thus, the full spike protein of any SARS-CoV-2 mutant is represented by a 1273-character sequence using this four-letter alphabet. Note that for regions outside the RBD, only the symbols 0 and 1 are used.

2.2 Cladogram algorithm on the construction of the cladogenetic tree

In the four-letter representation of mutants, let p_a denote the probability of a letter "a" (where $a \in \{0,1,2,3\}$) occurring in a sequence, and let p_{ab} represent the joint probability of consecutive occurrence of letters "a" and "b". More generally, for any n -letter segment $\sigma = abc\dots$, let p_σ denote the joint probability of the bases in σ occurring in the sequence. For joint probability calculations, all sequences are assumed to be circular. For any given n , the sum of joint probabilities over all segments σ of length n equals 1:

$$\sum_{\sigma} p_{\sigma} = 1,$$

where the summation extends over all 4^n possible segments of length n .

For two sequences Σ and Σ' with corresponding joint probability sets $\{p_{\sigma}\}$ and $\{p'_{\sigma}\}$, we define the n -mer distance between them based on joint probability differences as:

$$E_n(\Sigma, \Sigma') = \sum_{\sigma} |p_{\sigma} - p'_{\sigma}|. \quad n=1,2,\dots \quad (1)$$

The arguments of E_n may be omitted when unambiguous. This n -mer distance is well-defined for unaligned sequences of unequal lengths. By iteratively applying the relation:

$$|p_{\sigma} - p'_{\sigma}| = |\sum_a (p_{\sigma a} - p'_{\sigma a})| \leq \sum_a |p_{\sigma a} - p'_{\sigma a}|, \quad (2)$$

where σ is any n -letter segment and σa denotes an $(n+1)$ -letter segment, it follows that:

$$E_{n+1} \geq E_n, \quad n=1,2,\dots \quad (3)$$

Three primary algorithms are commonly employed for phylogenetic tree inference: distance matrix methods, maximum parsimony analysis, and maximum likelihood estimation [21]. In this study, we utilized these approaches (primarily the unweighted pair group method with arithmetic mean, UPGMA [22]) to reconstruct cladogenetic relationships.

3 Results and Discussion

3.1 Reconstruction of the cladogram of virus mutations

Without loss of generality, we constructed a distance matrix D for the 25 SARS-CoV-2 variants listed in Supplementary Material 1, Table S1 using the n -mer distance method. In this matrix, mutants are labeled as i, j, k, \dots , and each element D_{ij} represents the n -mer distance between sequences Σ_i and Σ_j , where Σ_i denotes the sequence of mutant i . By applying the UPGMA algorithm to this matrix, we reconstructed an evolutionary tree of the 25 mutants for a specific n . We observed that the cladogram structure stabilizes after several iterations as n increases, reaching a stable state when $n \geq 7$ [17]. Detailed comparisons of tree topologies for different n values are provided in Supplementary Material 2, Figures S1 and S2. Figure 1 displays the cladogram for $n = 7$, illustrating viral mutations in both four-letter and two-letter representations.

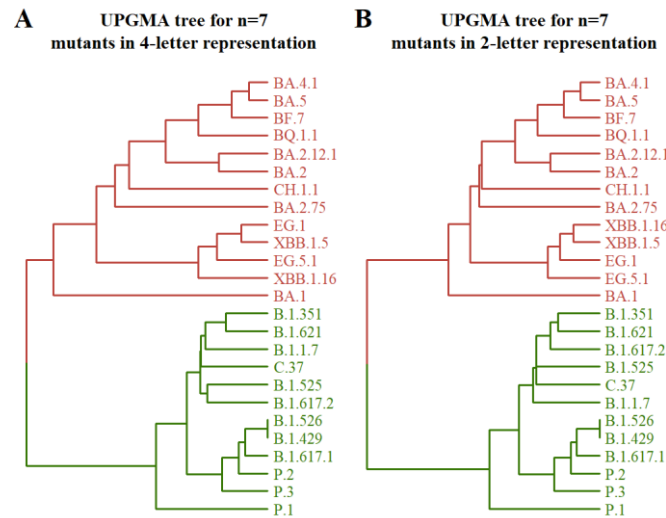


Fig. 1. Cladogenetic tree describing virus mutation. (A) The mutants in 4-letter representation. (B) The mutants in 2-letter representation (2-letter representation is the approximation of 4-letter representation and the related explanation can be found in the following text.)

In Figure 1, two major branches correspond to the macro-lineages N and O of the virus strains. Within macro-lineage O, sub-branches clearly show the divergence of BA.1 into BA.2, BA.4, and BA.5. The bifurcation of BA.1 from other O-lineage strains is consistent with recent phylogenetic analyses from Nextstrain [23]. Additionally, XBB is accurately classified as a recombinant of two BA.2 strains. In macro-lineage N, the sub-branch encompasses four variants of concern (VOCs): B.1.1.7 (Alpha), B.1.351 (Beta), B.1.617.2 (Delta), and P.1 (Gamma), each representing independent sub-lineages. These findings confirm that the theoretical tree aligns with

established evolutionary characteristics of the virus strains [6].

The tree reconstruction relies on two key assumptions: the four-letter representation of mutants and the n -mer distance algorithm. The four-letter scheme uses binary values (0 and 1) for 104 mutational sites on the spike protein, with two additional options (2 and 3) permitted at 27 sites in the receptor-binding domain (RBD). To simplify computations, we approximated this representation using a two-letter version, ignoring options 2 and 3. A comparison between the two-letter and four-letter representations for the 25 mutants is presented in Figure 1. Further structural comparisons of the cladograms are available in Supplementary Material 2.

Why does the two-letter representation approximate the four-letter version effectively? Due to interactions between the RBD and the human ACE-2 receptor, the 201 amino acid residues in the RBD cannot vary independently [13]. This constraint significantly reduces the informational complexity of the RBD. Thus, the two-letter approximation—which omits options 2 and 3 in the RBD—provides a reasonable simplification.

3.2 Generation of new strains on the cladogenetic tree using a stochastic method

Once the cladogenetic tree is constructed from known viral mutant lineages, new strains can be generated and analyzed within this framework. This section introduces a stochastic modeling approach for this process. Let set A comprise all mutated sites in updated virus strains, where a denotes the number of such sites. Each strain is represented as a two-letter sequence derived from $A(a)$.

To model stochastic mutations on the spike protein, let X denote a set of x sites subject to stochastic sampling. The union of sets $A(a)$ and $X(x)$ is defined as $Z = A \cup X$, while their intersection, containing y sites, is denoted $Y(y)$. Assuming that new strains arise from stochastic sampling within Z , each new strain is represented by a two-letter sequence from $Z(\text{len})$, where $\text{len} = a + x - y$. Using a cladogram algorithm, we reconstruct the cladogenetic tree of mutants in set Z , which incorporates the predicted new strain. This methodology is termed the A–X model [17].

Importantly, the model can consistently predict new strains, regardless of how sets A and X are distributed along the sequence or how set Y is incorporated. It ensures accurate predictions even with the continuous addition of new experimental data.

To demonstrate the feasibility of the A–X model in predicting new SARS-CoV-2 strains, we consider the example of 25 mutants listed in Supplementary Material 1, Table S1. Assume the evolutionary tree of these 25 mutants (set A) has two main branches, N and O. By performing stochastic sampling S times (e.g., $S = 10^5$), we generate 10^5 predictions for new strains. The following observations are made:

1. The new strain may belong to either branch N or O, or lie outside both, suggesting the emergence of a new macro-lineage.
2. For a fixed x , different values of y can lead to distinct predictions regarding the position of the new strain on the tree. The position is determined by the pair (x, y) . Thus, for a given (x, y) , the

predicted new strain is denoted as $New_{x,y}$.

3. When x is small, the predicted new strain typically falls within branch N or O. However, once x exceeds a certain threshold, an anomaly occurs, indicating the emergence of a new macro-lineage to which the new strain belongs.

3.3 Expanding the scope of stochastic sampling and predicting new SARS-CoV-2 macro-lineages

The emergence of new strains in phylogenetic trees is a stochastic process. As the scale of stochastic sampling expands, discernible statistical patterns begin to emerge. To broaden this sampling scope, we increased the size of x and randomized parameter y within the intersection set. This approach effectively enhances stochastic information, thereby facilitating new insights into the emergence of macro-lineages.

Generation of multiple macro-lineages

At a given time t , the emergence of new variants from set $A(a)$ can be predicted. In the A–X model, set X is stochastically selected, resulting in the random appearance of new variants on the phylogenetic tree. Nevertheless, the generation of multiple macro-lineages and the consequent bifurcation of the tree topology into several major branches are inevitable.

For example, at $t = T_1$ (October 15, 2023; accession date of 25 mutants; see Table S1 in Supplementary Material 1), we performed 10^5 rounds of stochastic sampling for x and 6 rounds of randomization for y . Throughout this process, the consistent emergence of macro-lineages N, O, and P was observed. The probability of a lineage (N, O, or P) for a given x is calculated as the occurrence count of that lineage divided by the total number of variants (10^5). Specifically, the macro-lineage affiliation of a newly generated variant is determined by its position within the bifurcated phylogenetic tree. The results are shown in Fig. 2, which plots the probability of the j -lineage ($j = N, O, P$) against x .

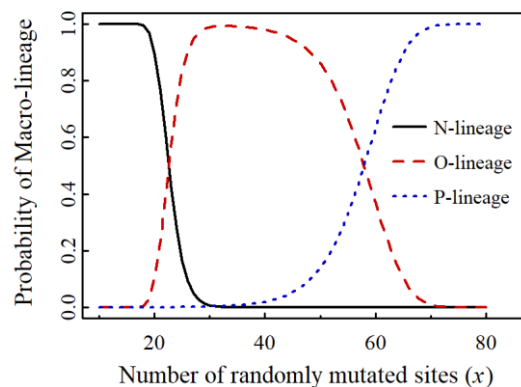


Fig. 2. PML(Probability of Macro-lineage) vs x for 25 mutants ($a=104$)

A 99th percentile threshold was used in the calculation. We found that the macro-lineage assignment of a new variant depends statistically on x , with specific threshold values distinguishing different macro-lineages as follows:

$New_{x,y} \in N$ when $x \leq 18$; $New_{x,y} \in N$ or O when $18 < x \leq 29$; $New_{x,y} \in O$ when $29 < x \leq 36$; $New_{x,y} \in O$ or P when $36 < x \leq 69$; and $New_{x,y} \in P$ when $x > 69$.

At a later time point, T_2 (July 20, 2024), after incorporating 11 new mutants (listed in Table S2 of Supplementary Material 1) into set A , the value of a increased from 104 to 128, covering 36 mutants in total. We repeated the stochastic sampling process with 10^5 iterations for x and 6 for y . The probabilities of each j -lineage ($j = N, O, P, Q$) are presented in Fig. 3.

Using the same method, we obtained the following threshold values of x for the case of 36 mutants:

$New_{x,y} \in N$ when $x \leq 18$; $New_{x,y} \in N$ or O when $18 < x \leq 29$; $New_{x,y} \in O$ when $29 < x \leq 39$; $New_{x,y} \in O$ or P when $39 < x \leq 62$; $New_{x,y} \in P$ when $62 < x \leq 72$; $New_{x,y} \in P$ or Q when $72 < x \leq 99$ and $New_{x,y} \in Q$ when $x > 99$.

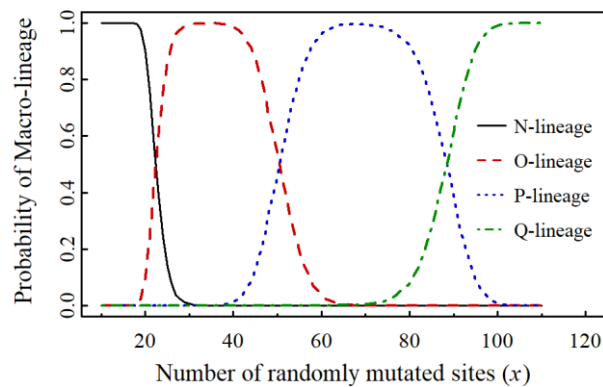


Fig. 3. PML(Probability of Macro-lineage) vs x for 36 mutants ($a=128$)

At the subsequent time point T_3 (January 4, 2025), after incorporating 70 variants from Table S3 into set A , the value of a increased to 153. The probabilities for each j -lineage ($j = N, O, P, Q$) based on these 70 mutants are shown in Fig. 4. The corresponding threshold values of x are defined as follows:

$New_{x,y} \in N$ when $x \leq 21$; $New_{x,y} \in N$ or O when $21 < x \leq 30$; $New_{x,y} \in O$ when $30 < x \leq 37$; $New_{x,y} \in O$ or P when $37 < x \leq 61$; $New_{x,y} \in P$ when $61 < x \leq 84$; $New_{x,y} \in P$ or Q when $84 < x \leq 112$ and $New_{x,y} \in Q$ when $x > 112$.

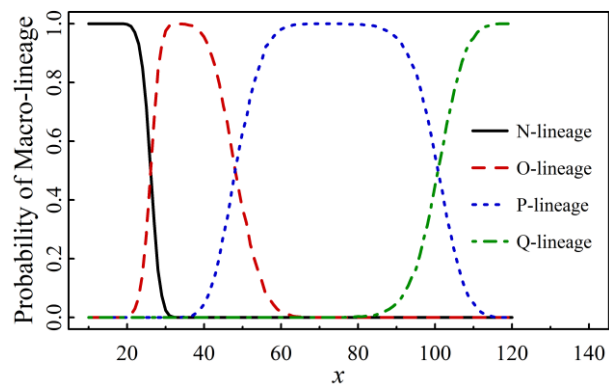


Fig. 4. PML(Probability of Macro-lineage) vs x for 70 mutants ($a=153$) given in Table S3

Law for the emergence of novel macro-lineages

Set $A(a)$ is an observable set dependent on time t . Set X represents a set of assumed mutated sites, also time-dependent, which is used to predict new macro-lineages. We define x_{dem1} as the threshold value of x at which a new macro-lineage emerges with a nonzero probability (greater than 1% in our calculations), and x_{dem2} as the threshold for its definitive occurrence. Both x_{dem1} and x_{dem2} are functions of time t .

At time t_k , the value of a is denoted as a_k , with examples including $a_1 = 104$, $a_2 = 128$ and $a_3 = 153$. The value of x_{dem1} for macro-lineage j (where $j = \text{O, P, Q}$) at time t_k is denoted as $x_{\text{dem1}}^{(j)}(t_k)$, and similarly, x_{dem2} for macro-lineage j at time t_k is denoted as $x_{\text{dem2}}^{(j)}(t_k)$. The values of $x_{\text{dem1}}^{(j)}(t_k)$ and $x_{\text{dem2}}^{(j)}(t_k)$ are presented in Figs. 2–4 and summarized in Table 1.

Table 1. Demarcation values x_{dem1} and x_{dem2} at three times t_1 and t_2 and t_3

k	a_k	$x_{\text{dem1}}^{(\text{O})}(t_k)$	$x_{\text{dem2}}^{(\text{O})}(t_k)$	$x_{\text{dem1}}^{(\text{P})}(t_k)$	$x_{\text{dem2}}^{(\text{P})}(t_k)$	$x_{\text{dem1}}^{(\text{Q})}(t_k)$	$x_{\text{dem2}}^{(\text{Q})}(t_k)$
1	104	19	30	37	70	-	-
2	128	19	30	40	63	73	100
3	153	22	31	38	62	85	113

Note: $t_1 < t_2 < t_3$. t_1 is the time period later than $T_1 = \text{October 15, 2023}$, t_2 is the time period later than $T_2 = \text{July 20, 2024}$, t_3 is the time period later than $T_3 = \text{January 4, 2025}$. The starting point for each time period can be found in Supplementary Table S1, S2 and S3 respectively.

Table 1 outlines the occurrence pattern of novel macro-lineages: the O-lineage emerges at $x \approx 19$ –22 and definitively occurs at $x \approx 30$ –31; the P-lineage emerges at $x \approx 37$ –40 and definitively occurs at $x \approx 62$ –70; the Q-lineage emerges at $x \approx 73$ –85 and definitively occurs at $x \approx 100$ –113. The threshold values deduced across different time periods are highly consistent.

Based on Table 1 and Fig. 2, we predicted the emergence of the P-lineage at time t_1 . However, no P-lineage is observed in the cladogenetic tree for 25 mutants (see Fig. 1 and Supplementary Figure S1). The P-lineage appears in the cladogenetic tree only when the number of mutants reaches 36 or more. This suggests that our prediction preceded the actual observation and phylogenetic confirmation.

From Table 1 and Figs. 3–4, we predicted the emergence of a new Q-lineage from the P-lineage at a sufficiently high x value (exceeding 73–85). Notably, the number of mutated sites (x) in the P-lineage never exceeded 68, as shown in Table S3. However, in Table S4, we identified a new variant, BA.3.2.2, with 74 mutated sites. To investigate whether BA.3.2.2 is associated with the emergence of a new lineage, we constructed a phylogenetic tree using a cladogenesis algorithm (Fig. 5).

Fig. 5 reveals that most new variants belong to the P-lineage, whereas BA.3.2.2 has diverged from it. Therefore, we hypothesize that the occurrence of BA.3.2.2 in April 2025 may signal the emergence of the new Q-lineage. This prediction warrants further validation in the near future.

In conclusion, by conceptualizing stochastic mutation as a mechanism driving the emergence of new SARS-CoV-2 variants, we derived a principle governing macro-lineage transformation from N to P and then to Q. This approach offers a predictive framework for anticipating the future dominance of novel SARS-CoV-2 variants.

UPGMA tree for $n=7$
mutants in 2-letter representation

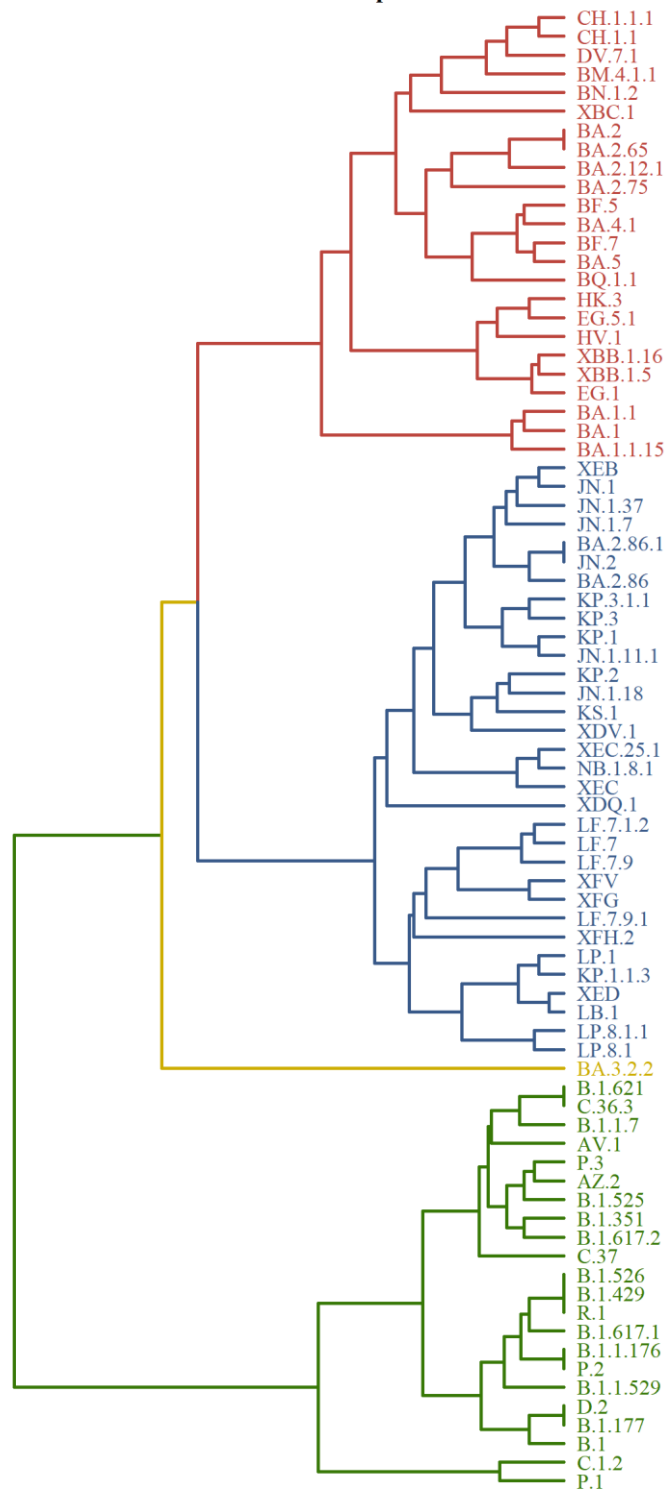


Fig. 5. UPGMA tree of $n=7$ in 2-letter representation for 79 mutants by taking new variants (in Next Strain, see Table S4) into account

3.4 Each macro-lineage of SARS-CoV-2 has a specific survival time

The relationship between the number of mutated sites and time t is a discontinuous function

According to the retrieval of SARS-CoV-2 variant data in Table S3, Table S5 presents the relationship between the number of mutated sites (NMS) in the spike protein and the initial global sample collection dates for each SARS-CoV-2 variant, arranged chronologically. Our analysis reveals that $NMS(t)$ represents a discontinuous function of time, corresponding to three distinct macro-lineages (Fig. 6A). This figure is derived directly from the data in Table S5.

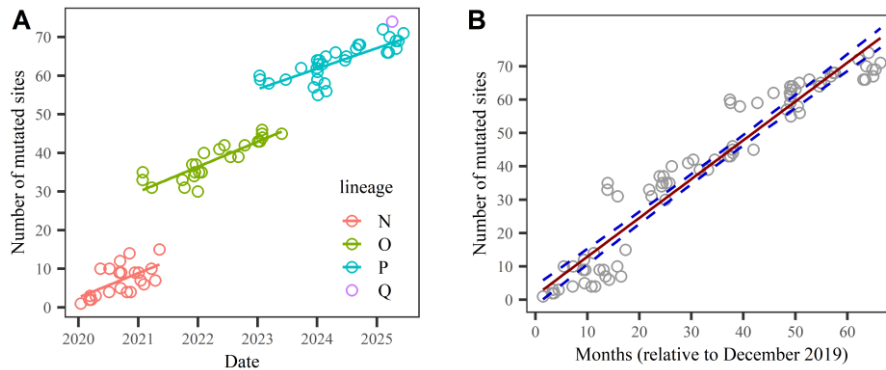


Fig. 6. (A) Number of mutated sites versus the initial sample collection date. (B) Linear regression analysis of mutated site counts against initial sample collection dates, with 95% confidence intervals (represented by blue dotted lines) calculated using linear regression theory.

Linear regression of mutated sites vs. sample collection date as an approximation

We performed linear regression to analyze the relationship between the number of mutated sites and the initial sample collection date; the results are shown in Fig. 6B. The linear model effectively captures the increasing trend in mutated sites over viral evolution. The regression yielded an R^2 value of 0.92 and an RSE (Residual Standard Error) of 6.68. Furthermore, using linear regression theory, we estimated a slope of 1.163 per month (95% CI: ± 0.076). Given the strong fit of this linear model, we will utilize the relationship between the number of mutated sites (x) and collection time (t) to predict the emergence of new viral lineages.

Why does the number of mutated sites increase approximately linearly with emergence time? As shown in Fig. 6A, the relationship between the number of mutated sites (NMS) and time (t) is discontinuous and exhibits stepwise changes at lineage transformation points. However, the slope of NMS increase differs between adjacent lineages. Typically, newer lineages show a lower rate of increase than older ones, offsetting the stepwise changes during lineage transformation. This compensatory mechanism accounts for the overall approximately linear relationship between NMS and emergence time. Our prediction for the new lineage relies on extrapolating this linear trend over an extended period.

Prediction of the emergence time of the possible Q macro-lineage

Based on the above analyses, we propose an algorithm for predicting the emergence timeline of macro-lineages. In the A–X model, the number of randomly mutated sites for a variant is denoted as x . Notably, $NMS(t)$, which quantifies the accumulation of mutated sites over time, is intrinsically related to x . Using the data from Fig. 4—which shows the relationship between the probability of macro-lineage emergence (PML) and x , as well as the time dependence of

NMS(t)—we predict the emergence time of the new macro-lineage Q. By extrapolating the linear trend over a longer period and applying linear regression, we estimate that the number of mutated sites will reach $NMS = 73.4 \pm 2.6$ to 85 ± 3 between the 62nd and 72nd months, and 100 ± 4 to 113 ± 5 between the 85th and 96th months, starting from December 2019. Combining these values with the thresholds $x_{dem1} = 73-85$ (indicating the initial emergence of Q) and $x_{dem2} = 100-113$ (indicating a major outbreak of Q), we preliminarily predict that macro-lineage Q will emerge around February to December 2025, and may experience a strong outbreak approximately 22 to 24 months later. Currently, the new variant BA.3.2.2, which emerged in April 2025, appears to signal the initial rise of macro-lineage Q (Fig. 5). However, since the mutation probabilities of sites on the spike protein are strongly influenced by diverse biological driving forces, the actual timeline for macro-lineage emergence may differ. Thus, the above estimation should be used for reference only.

Conclusions

COVID-19 has spread globally through successive waves of infection. Two distinct patterns of pandemic propagation have been observed: one involves recurrent outbreaks of existing strains [18], while the other entails the emergence of novel variants. This study focuses specifically on the latter pattern.

1. Using the cladogram algorithm and the A–X model [17]—where Set A comprises existing mutated sites and Set X contains x randomly generated sites on the spike protein—we can investigate the relationship between stochastic mutations and the generation of new strains within a cladogram framework.
2. Based on the understanding that stochastic mutation drives the emergence of new SARS-CoV-2 variants, we deduced a principle governing macro-lineage transformation. By expanding the scope of stochastic sampling, we demonstrate that a new macro-lineage emerges alongside existing lineages once the number of randomly generated sites (x) reaches a critical threshold. As x increases further, the relative proportions of the four macro-lineages shift: O surpasses N, P subsequently surpasses O, and finally, a new lineage Q may emerge. This principle offers a novel approach for predicting the future dominance of new SARS-CoV-2 variants.
3. Based on the linear regression of the number of mutated sites per variant against its global initial sampling time, we propose an algorithm for predicting the emergence timeline of macro-lineages. By incorporating the influence of diverse biological drivers on spike protein mutation probabilities, this algorithm facilitates more accurate predictions of the actual emergence timing of new macro-lineages.

Author statements

Author contributions

L. L.: conceptualization, methodology, writing – original draft and writing - review & editing. J. L.: methodology, visualization, validation and writing - review & editing.

Conflicts of interest

The author(s) declare that there are no conflicts of interest.

Funding information

This work received no specific grant from any funding agency.

Ethical approval

Not applicable.

Consent for publication

Not applicable.

Acknowledgements

We sincerely appreciate Dr. Ying Zhang for her assistance with data collection, insightful discussions, and valuable suggestions.

References

1. **Carabelli AM, Peacock TP, Thorne LG, Harvey WT, Hughes J, et al.** SARS-CoV-2 variant biology: immune escape, transmission and fitness. *Nat Rev Microbiol* 2023; 21:162-177. <https://doi.org/10.1038/s41579-022-00841-7>.
2. **Markov PV, Ghafari M, Beer M, Lythgoe K, Simmonds P, et al.** The evolution of SARS-CoV-2. *Nat Rev Microbiol.* 2023; 21:361-379. <https://doi.org/10.1038/s41579-023-00878-2>.
3. **Cao Y, Jian F, Wang J, Yu Y, Song W, et al.** Imprinted SARS-CoV-2 humoral immunity induces convergent Omicron RBD evolution. *Nature* 2023; 614:521-529. <https://doi.org/10.1038/s41586-022-05644-7>.
4. **Mallapaty S.** Where did Omicron come from? Three key theories. *Nature* 2022; 602: 26-28. <https://doi.org/10.1038/d41586-022-00215-2>.
5. **Callaway E.** Beyond Omicron: what's next for COVID's viral evolution. *Nature* 2021; 600: 204-207. <https://doi.org/10.1038/d41586-021-03619-8>.
6. **Wang Q, Iketani S, Li Z, Liu L, Guo Y, et al.** Alarming antibody evasion properties of rising SARS-CoV-2 BQ and XBB subvariants. *Cell* 2023; 186: 279-286.e8. <https://doi.org/10.1016/j.cell.2022.12.018>.
7. **Rahnsch B, Taghizadeh L.** Network-based uncertainty quantification for mathematical models in epidemiology. *J Theor Biol* 2024; 577: 111671. <https://doi.org/10.1016/j.jtbi.2023.111671>.
8. **Ramachandran A, Lumetta SS, Chen D.** PandoGen: Generating complete instances of future SARS-CoV-2 sequences using Deep Learning. *PLoS Comput Biol* 2024; 20: e1011790. <https://doi.org/10.1371/journal.pcbi.1011790>.
9. **Fowler DM, Fields S.** Deep mutational scanning: a new style of protein science. *Nat Methods* 2014; 11: 801-807. <https://doi.org/10.1038/nmeth.3027>.

10. **Elnaggar A, Heinzinger M, Dallago C, Rehawi G, Wang Y, et al.** ProtTrans: Toward understanding the language of life through self-supervised learning. *IEEE Trans Pattern Anal Mach Intell* 2022; 44: 7112-7127. <https://doi.org/10.1109/TPAMI.2021.3095381>.
11. **Ferruz N, Schmidt S, Höcker B.** ProtGPT2 is a deep unsupervised language model for protein design. *Nat Commun* 2022; 13: 4348. <https://doi.org/10.1038/s41467-022-32007-7>.
12. **Ma W, Fu H, Jian F, Cao Y, Li M.** Immune evasion and ACE2 binding affinity contribute to SARS-CoV-2 evolution. *Nat Ecol Evol* 2023; 7: 1457-1466. <https://doi.org/10.1038/s41559-023-02123-8>.
13. **Sultana N, Nagesha SN, Reddy CNL, Ramesh BN, Shyamamma S, et al.** Computational analysis of affinity dynamics between the variants of SARS-CoV-2 spike protein (RBD) and human ACE-2 receptor. *Virology* 2024; 21: 88. <https://doi.org/10.1186/s12985-024-02365-3>
14. **Yao Z, Zhang L, Duan Y, Tang X, Lu J.** Molecular insights into the adaptive evolution of SARS-CoV-2 spike protein. *J Infect* 2024; 88: 106121. <https://doi.org/10.1016/j.jinf.2024.106121>.
15. **Ma E, Guo X, Hu M, Wang P, Wang X, et al.** A predictive language model for SARS-CoV-2 evolution. *Sig Transduct Target Ther* 2024; 9: 353. <https://doi.org/10.1038/s41392-024-02066-x>.
16. **Guo C, Yu Y, Liu J, Jian F, Yang S, et al.** Antigenic and virological characteristics of SARS-CoV-2 variants BA.3.2, XFG, and NB.1.8.1. *Lancet Infect Dis* 2025; 25: e374-e377. [https://doi.org/10.1016/S1473-3099\(25\)00308-1](https://doi.org/10.1016/S1473-3099(25)00308-1).
17. **Luo L, Lv J.** An evolutionary theory on virus mutation in COVID-19. *Virus Res* 2024; 344: 199358. <https://doi.org/10.1016/j.virusres.2024.199358>.
18. **Luo L, Lv J.** Mathematical modelling of virus spreading in COVID-19. *Viruses* 2023; 15: 1788. <https://doi.org/10.3390/v15091788>.
19. **Gangavarapu K, Latif AA, Mullen JL, Alkuzweny M, Hufbauer E, et al.** Outbreak.info genomic reports: scalable and dynamic surveillance of SARS-CoV-2 variants and mutations. *Nat Methods* 2023; 20: 512-522. <https://doi.org/10.1038/s41592-023-01769-3>.
20. **Starr TN, Greaney AJ, Hilton SK, Ellis D, Crawford KHD, et al.** Deep mutational scanning of SARS-CoV-2 receptor binding domain reveals constraints on folding and ACE2 binding. *Cell* 2020; 182: 1295-1310.e20. <https://doi.org/10.1016/j.cell.2020.08.012>.
21. **Li W-H.** *Molecular evolution* Sinauer Associates; 1997.
22. **Nei M, Kumar S.** *Molecular evolution and phylogenetics* Oxford University Press; 2000.
23. **Hadfield J, Megill C, Bell SM, Huddleston J, Potter B, et al.** Nextstrain: real-time tracking of pathogen evolution. *Bioinformatics* 2018; 34: 4121-4123. <https://doi.org/10.1093/bioinformatics/bty407>.

Supplementary Material:

Stochastic Mutation as a Mechanism for the Emergence of

SARS-CoV-2 New Variants

Liaofu Luo^{1*}, Jun Lv^{2*}

¹Faculty of Physical Science and Technology, Inner Mongolia University, 235 West College Road, Hohhot 010021, PR China

²College of Science, Inner Mongolia University of Technology, 49 Aymin Street, Hohhot 010051, PR China

*Correspondence:

Liaofu Luo

lolfcm@imu.edu.cn

Jun Lv

lujun@imut.edu.cn

Supplementary Material 1: Mutation data of SARS-CoV-2 Variants

Table S1 Partial table of 25 variants and their mutation sites

A total of 25 variants from the mutation reports provided by outbreak.info (<https://outbreak.info/>, accessed on 15 October 2023)

macro-lineage	No	variant	NM	mutated sites
ge	.		S	
N-lineage	1	P.2(Zeta)	3	484,614,1176
	2	B.1.1.7(Alpha)	10	69,70,144, 501 ,570,614,681,716,982,1118
	3	B.1.429(Epsilon)	4	13,152, 452,614
	4	B.1.351(Beta)	10	80,215,241,242,243, 417,484,501 ,614,701
	5	B.1.617.2(Delta)	9	19,156,157,158, 452,478 ,614,681,950
	6	P.1(Gamma)	12	18,20,26,138,190, 417,484,501 ,614,655,1027,1176
	7	B.1.617.1(Kappa)	5	452,484 ,614,681,1071
	8	B.1.621(Mu)	9	95,144,145, 346,484,501 ,614,681,950
	9	C.37(Lambda)	14	75,76,246,247,248,249,250,251,252,253, 452,490 ,614,859
	10	B.1.526(Iota)	4	5,95,253,614
	11	B.1.525(Eta)	9	52,67,69,70,144, 484 ,614,677,888
	12	P.3(Theta)	7	484,501 ,614,681,1092,1101,1176
O-lineage	13	BA.1	33	67,69,70,95,142,143,144,145,211,212, 339,371,373,375,477,478,484,493,496,498,501,505 ,547,614,655,679,681,764,796,856,954,969,981
	14	BA.2	31	19,24,25,26,27,142,213, 339,371,373,375,376,405,408,417,440,477,478,484,493,498,501,505 ,614,655,679,681,764,796,954,969

15	BA.2.12.1	33	19,24,25,26,27,142,213, 339,371,373,375,376,405,408,417,440,452,477,478,484,493,498,501,505 ,614,655,679,681,704,764,796,954,969
16	BA.5	34	19,24,25,26,27,69,70,142,213, 339,371,373,375,376,405,408,417,440,452,477,478,484,486,498,501,505 ,614,655,679,681,764,796,954,969
17	BA.4.1	35	3,19,24,25,26,27,69,70,142,213, 339,371,373,375,376,405,408,417,440,452,477,478,484,486,498,501,505 ,614,655,679,681,764,796,954,969
18	BQ.1.1	37	19,24,25,26,27,69,70,142,213, 339,346,371,373,375,376,405,408,417,440,444,452,460,477,478,484,486,498,501,505 ,614,655,679,681,764,796,954,969
19	BA.2.75	30	19,24,210,213,257, 339,371,373,375,376,405,408,417,440,446,460,477,478,484,498,501,505 ,614,655,679,681,764,796,954,969
20	BF.7	35	19,24,25,26,27,69,70,142,213, 339,346,371,373,375,376,405,408,417,440,452,477,478,484,486,498,501,505 ,614,655,679,681,764,796,954,969
21	CH.1.1	41	19,24,25,26,27,142,147,152,157,210,213,257, 339,346,371,373,375,376,405,408,417,440,444,446,452,460,477,478,484,486,498,501,505 ,614,655,679,681,764,796,954,969
22	XBB.1.5	42	19,24,25,26,27,83,142,144,146,183,213,252, 339,346,368,371,373,375,376,405,408,417,440,445,446,460,477,478,484,486,490,498,501,505 ,614,655,679,681,764,796,954,969
23	XBB.1.16	43	19,24,25,26,27,83,142,144,146,180,183,213,252, 339,346,368,371,373,375,376,405,408,417,440,445,446,460,477,478,484,486,490,498,501,505 ,614,655,679,681,764,796,954,969
24	EG.1	43	19,24,25,26,27,83,142,144,146,183,213,252, 339,346,368,371,373,375,376,405,408,417,440,445,446,460,477,478,484,486,490,498,501,505 ,613,614,655,679,681,764,796,954,969
25	EG.5.1	44	19,24,25,26,27,52,83,142,144,146,183,213,252, 339,346,368,371,373,375,376,405,408,417,440,445,446,456,460,477,478,484,486,490,498,501,505 ,614,655,679,681,764,796,954,969
total		104	3, 5, 13, 18, 19, 20, 24, 25, 26, 27, 52, 67, 69, 70, 75, 76, 80, 83, 95, 138, 142, 143, 144, 145, 146, 147, 152, 156, 157, 158, 180, 183, 190, 210, 211, 212, 213, 215, 241, 242, 243, 246, 247, 248, 249, 250, 251, 252, 253, 257, 339, 346, 368, 371, 373, 375, 376, 405, 408, 417, 440, 444, 445, 446, 452, 456, 460, 477, 478, 484, 486, 490, 493, 496, 498, 501, 505 , 547, 570, 613, 614, 655, 677, 679, 681, 701, 704, 716, 764, 796, 856, 859, 888, 950, 954, 969, 981, 982, 1027, 1071, 1092, 1101, 1118, 1176

NMS: number of mutated sites; Mutated sites are considered when they occur in at least 75% of the SARS-CoV-2 lineage sequences. Mutations in the spike protein's receptor-binding domain (RBD) are indicated in bold.

Table S2 Partial table of 36 variants and their mutation sites

A total of 36 variants from the mutation reports provided by outbreak.info (<https://outbreak.info/>, accessed on 20 July 2024)

macro-lineage	No	variant	NM	mutated sites
ge	.		S	
N-lineage	1	P.2(Zeta)	3	484,614,1176
	2	B.1.1.7(Alpha)	10	69,70,144, 501 ,570,614,681,716,982,1118
	3	B.1.429(Epsilon)	4	13,152, 452 ,614
	4	B.1.351(Beta)	10	80,215,241,242,243, 417,484,501 ,614,701
	5	B.1.617.2(Delta)	9	19,156,157,158, 452,478 ,614,681,950
	6	P.1(Gamma)	12	18,20,26,138,190, 417,484,501 ,614,655,1027,1176
	7	B.1.617.1(Kappa)	5	452,484 ,614,681,1071
	8	B.1.621(Mu)	9	95,144,145, 346,484,501 ,614,681,950
	9	C.37(Lambda)	14	75,76,246,247,248,249,250,251,252,253, 452,490 ,614,859
	10	B.1.526(Iota)	4	5,95,253,614
	11	B.1.525(Eta)	9	52,67,69,70,144, 484 ,614,677,888
	12	P.3(Theta)	7	484,501 ,614,681,1092,1101,1176
O-lineage	13	BA.1	33	67,69,70,95,142,143,144,145,211,212, 339,371,373,375,477,478,484,493,496,498,501,505 ,547,614,655,679,681,764,796,856,954,969,981
	14	BA.2	31	19,24,25,26,27,142,213, 339,371,373,375,376,405,408,417,440,477,478,484,493,498,501,505 ,614,655,679,681,764,796,954,969
	15	BA.2.12.1	33	19,24,25,26,27,142,213, 339,371,373,375,376,405,408,417,440,452,477,478,484,493,498,501,505 ,614,655,679,681,704,764,796,954,969
	16	BA.5	34	19,24,25,26,27,69,70,142,213, 339,371,373,375,376,405,408,417,440,452,477,478,484,486,498,501,505 ,614,655,679,681,764,796,954,969
	17	BA.4.1	35	3,19,24,25,26,27,69,70,142,213, 339,371,373,375,376,405,408,417,440,452,477,478,484,486,498,501,505 ,614,655,679,681,764,796,954,969
	18	BQ.1.1	37	19,24,25,26,27,69,70,142,213, 339,346,371,373,375,376,405,408,417,440,444,452,460,477,478,484,486,498,501,505 ,614,655,679,681,764,796,954,969
	19	BA.2.75	30	19,24,210,213,257, 339,371,373,375,376,405,408,417,440,446,460,477,478,484,486,498,501,505 ,614,655,679,681,764,796,954,969
	20	BF.7	35	19,24,25,26,27,69,70,142,213, 339,346,371,373,375,376,405,408,417,440,452,477,478,484,486,498,501,505 ,614,655,679,681,764,796,954,969
	21	CH.1.1	41	19,24,25,26,27,142,147,152,157,210,213,257, 339,346,371,373,375,376,405,408,417,440,444,446,452,460,477,478,484,486,498,501,505 ,614,655,679,681,764,796,954,969
	22	XBB.1.5	42	19,24,25,26,27,83,142,144,146,183,213,252, 339,346,368,371,373,375,376,405,408,417,440,445,446,460,477,478,484,486,490,498,501,505 ,614,655,679,681,764,796,954,969
	23	XBB.1.16	43	19,24,25,26,27,83,142,144,146,180,183,213,252, 339,346,368,371,373,375,376,405,408,417,440,445,446,460,477,478,484,486,490,498,501,505 ,614,655,679,681,764,796,954,969
	24	EG.1	43	19,24,25,26,27,83,142,144,146,183,213,252, 339,346,368,371,373,375,376,405,408,417,440,445,446,460,477,478,484,486,490,498,501,505 ,613,614,655,679,681,764,796,954,969
	25	EG.5.1	44	19,24,25,26,27,52,83,142,144,146,183,213,252, 339,346,368,371,373,375,376,405,408,417,440,445,446,456,460,477,478,484,486,490,498,501,505 ,614,655,679,681,764,796,954,969
	26	HV.1	46	19,24,25,26,27,52,83,142,144,146,157,183,213,252, 339,346,

				368,371,373,375,376,405,408,417,440,445,446,452,456,460,477,478,484,486,490,498,501,505,614,655,679,681,764,796,954,969
P-lineage	27	JN.1	60	19,21,24,25,26,27,50,69,70,127,142,144,157,158,211,212,213,216,245,264, 332,339,356,371,373,375,376,403,405,408,417,440,445,446,450,452,455,460,477,478,481,483,484,486,498,501,505 ,554,570,614,621,655,679,681,764,796,939,954,969,1143
	28	BA.2.86.1	59	19,21,24,25,26,27,50,69,70,127,142,144,157,158,211,212,213,216,245,264, 332,339,356,371,373,375,376,403,405,408,417,440,445,446,450,452,460,477,478,481,483,484,486,498,501,505 ,554,570,614,621,655,679,681,764,796,939,954,969,1143
	29	BA.2.86	58	19,21,24,25,26,27,50,69,70,127,142,144,157,158,211,212,213,216,245,264, 332,339,356,371,373,375,376,403,405,408,417,440,445,446,450,452,460,477,478,481,484,486,498,501,505 ,554,570,614,621,655,679,681,764,796,939,954,969,1143
	30	JN.1.7	62	19,21,24,25,26,27,50,69,70,127,142,144,157,158,211,212,213,216,245,264, 332,339,356,371,373,375,376,403,405,408,417,440,445,446,450,452,455,460,477,478,481,483,484,486,498,501,505 ,554,570,572,614,621,655,679,681,764,796,939,954,969,1143,1150
	31	KP.3.1.1	64	19,21,24,25,26,27,31,50,69,70,127,142,144,157,158,211,212,213,216,245,264, 332,339,356,371,373,375,376,403,405,408,417,440,445,446,450,452,455,456,460,477,478,481,483,484,486,493,498,501,505 ,554,570,614,621,655,679,681,764,796,939,954,969,1104,1143
	32	KP.2	59	19,21,50,69,70,127,142,144,157,158,211,212,213,216,245,264, 332,339,346,356,371,373,375,376,403,405,408,417,440,445,446,450,452,455,456,460,477,478,481,483,484,486,498,501,505 ,554,570,614,621,655,679,681,764,796,939,954,969,1104,1143
	33	JN.1.37	61	19,21,24,25,26,27,50,69,70,127,142,144,157,158,211,212,213,216,245,264, 332,339,356,371,373,375,376,403,405,408,417,440,445,446,450,452,455,460,477,478,481,483,484,486,498,501,505 ,554,570,614,621,655,679,680,681,764,796,939,954,969,1143
	34	XDQ.1	55	19,21,24,25,26,27,50,69,70,127,142,144,157,158,211,212,213,216,245,264, 332,339,356,371,373,375,376,403,405,408,417,440,445,446,450,452,460,475,483,484,486,498,501,505 ,554,570,614,621,655,679,681,764,796,954,969
	35	LB.1	64	19,21,24,25,26,27,31,50,69,70,127,142,144,157,158,183,211,212,213,216,245,264, 332,339,346,356,371,373,375,376,403,405,408,417,440,445,446,450,452,455,456,460,477,478,481,483,484,486,498,501,505 ,554,570,614,621,655,679,681,764,796,939,954,969,1143
	36	KP.1	63	19,21,24,25,26,27,50,69,70,127,142,144,157,158,211,212,213,216,245,264, 332,339,356,371,373,375,376,403,405,408,417,440,445,446,450,452,455,456,460,477,478,481,483,484,486,498,501,505 ,547,554,570,572,613,614,621,655,677,679,680,681,701,704,716,764,796,856,859,888,939,950,954,969,981,982,1027,1071,1086,1092,1101,1104,1118,1143,1150,1176
total			128	3,5,13,18,19,20,21,24,25,26,27,31,50,52,67,69,70,75,76,80,83,95,127,138,142,143,144,145,146,147,152,156,157,158,180,183,190,210,211,212,213,215,216,241,242,243,245,246,247,248,249,250,251,252,253,257,264, 332,339,346,356,368,371,373,375,376,403,405,408,417,440,444,445,446,450,452,455,456,460,475,477,478,481,483,484,486,490,493,496,498,501,505 ,547,554,570,572,613,614,621,655,677,679,680,681,701,704,716,764,796,856,859,888,939,950,954,969,981,982,1027,1071,1086,1092,1101,1104,1118,1143,1150,1176

NMS: number of mutated sites; Mutated sites are considered when they occur in at least 75% of the SARS-CoV-2 lineage sequences. Mutations in the spike protein's receptor-binding domain (RBD) are indicated in bold.

Table S3 General table of 70 variants and their mutation sites

A total of 70 variants from the mutation reports provided by outbreak.info (<https://outbreak.info/>, accessed on 4 January 2025)

macro-lineage	No	variant	NM	mutated sites
ge	.		S	
N-lineage	1	B.1	1	614
	2	B.1.177	2	222,614
	3	B.1.1.176	3	20,357,614
	4	D.2	2	477,614
	5	P.2(Zeta)	3	484,614,1176
	6	B.1.1.7(Alpha)	10	69,70,144,501,570,614,681,716,982,1118
	7	B.1.429(Epsilon)	4	13,152,452,614
	8	B.1.351(Beta)	10	80,215,241,242,243,417,484,501,614,701
	9	B.1.617.2(Delta)	9	19,156,157,158,452,478,614,681,950
	10	P.1(Gamma)	12	18,20,26,138,190,417,484,501,614,655,1027,1176
	11	B.1.617.1(Kappa)	5	452,484,614,681,1071
	12	B.1.621(Mu)	9	95,144,145,346,484,501,614,681,950
	13	R.1	4	152,484,614,769
	14	C.37(Lambda)	14	75,76,246,247,248,249,250,251,252,253,452,490,614,859
	15	B.1.526(Iota)	4	5,95,253,614
	16	B.1.525(Eta)	9	52,67,69,70,144,484,614,677,888
	17	C.36.3	9	12,69,70,152,346,452,614,677,899
	18	P.3(Theta)	7	484,501,614,681,1092,1101,1176
	19	AZ.2	6	95,144,484,614,681,796
	20	AV.1	10	80,95,142,144,439,484,614,681,1130,1139
	21	B.1.1.529	7	373,478,614,655,679,681,954
	22	C.1.2	15	9,136,144,190,215,243,244,449,484,501,614,655,679,716,859
O-lineage	23	BA.1	33	67,69,70,95,142,143,144,145,211,212,339,371,373,375,477,478,484,493,496,498,501,505,547,614,655,679,681,764,796,856,954,969,981
	24	BA.1.1	35	67,69,70,95,142,143,144,145,211,212,339,346,371,373,375,446,477,478,484,493,496,498,501,505,547,614,655,679,681,764,796,856,954,969,981
	25	BA.2	31	19,24,25,26,27,142,213,339,371,373,375,376,405,408,417,440,477,478,484,493,498,501,505,614,655,679,681,764,796,954,969
	26	BA.2.12.1	33	19,24,25,26,27,142,213,339,371,373,375,376,405,408,417,440,452,477,478,484,493,498,501,505,614,655,679,681,704,764,796,954,969
	27	BA.2.65	31	19,24,25,26,27,142,213,339,371,373,375,376,405,408,417,440,477,478,484,493,498,501,505,614,655,679,681,764,796,954,969
	28	BA.1.1.15	37	67,69,70,95,142,143,144,145,211,212,339,346,371,373,375,417,440,446,477,478,484,493,496,498,501,505,547,614,655,679,681,764,796,856,954,969,981
	29	BA.5	34	19,24,25,26,27,69,70,142,213,339,371,373,375,376,405,408,417,440,452,477,478,484,486,498,501,505,614,655,679,681,764,796,954,969
	30	BA.4.1	35	3,19,24,25,26,27,69,70,142,213,339,371,373,375,376,405,408,417,440,452,477,478,484,486,498,501,505,614,655,679,681,764,796,954,969
	31	BQ.1.1	37	19,24,25,26,27,69,70,142,213,339,346,371,373,375,376,405,408,417,440,444,452,460,477,478,484,486,498,501,505,614,

			655,679,681,764,796,954,969	
	32	BA.2.75	30	19,24,210,213,257,339,371,373,375,376,405,408,417,440,446,460,477,478,484,498,501,505,614,655,679,681,764,796,954,969
	33	BF.5	35	19,24,25,26,27,69,70,142,213,339,371,373,375,376,405,408,417,440,452,477,478,484,486,498,501,505,614,655,679,681,764,796,954,969,1020
	34	BF.7	35	19,24,25,26,27,69,70,142,213,339,346,371,373,375,376,405,408,417,440,452,477,478,484,486,498,501,505,614,655,679,681,764,796,954,969
	35	BN.1.2	40	19,24,25,26,27,142,147,152,157,210,213,257,339,346,356,371,373,375,376,405,408,417,440,446,460,477,478,484,490,498,501,505,614,655,679,681,764,796,954,969
	36	CH.1.1	41	19,24,25,26,27,142,147,152,157,210,213,257,339,346,371,373,375,376,405,408,417,440,444,446,452,460,477,478,484,486,498,501,505,614,655,679,681,764,796,954,969
	37	XBB.1.5	42	19,24,25,26,27,83,142,144,146,183,213,252,339,346,368,371,373,375,376,405,408,417,440,445,446,460,477,478,484,486,490,498,501,505,614,655,679,681,764,796,954,969
	38	BM.4.1.1	39	19,24,25,26,27,142,147,152,157,210,213,257,339,346,371,373,375,376,405,408,417,440,446,460,477,478,484,486,498,501,505,614,655,679,681,764,796,954,969
	39	XBC.1	39	19,25,142,144,156,157,158,209,212,215,222,243,244,371,373,375,376,405,408,417,440,446,452,477,478,484,486,498,501,505,614,655,679,681,703,764,796,954,969
	40	CH.1.1.1	42	19,24,25,26,27,142,147,152,157,185,210,213,257,339,346,371,373,375,376,405,408,417,440,444,446,452,460,477,478,484,486,498,501,505,614,655,679,681,764,796,954,969
	41	XBB.1.16	43	19,24,25,26,27,83,142,144,146,180,183,213,252,339,346,368,371,373,375,376,405,408,417,440,445,446,460,477,478,484,486,490,498,501,505,614,655,679,681,764,796,954,969
	42	EG.1	43	19,24,25,26,27,83,142,144,146,183,213,252,339,346,368,371,373,375,376,405,408,417,440,445,446,460,477,478,484,486,490,498,501,505,613,614,655,679,681,764,796,954,969
	43	HV.1	46	19,24,25,26,27,52,83,142,144,146,157,183,213,252,339,346,368,371,373,375,376,405,408,417,440,445,446,452,456,460,477,478,484,486,490,498,501,505,614,655,679,681,764,796,954,969
	44	HK.3	45	19,24,25,26,27,52,83,142,144,146,183,213,252,339,346,368,371,373,375,376,405,408,417,440,445,446,455,456,460,477,478,484,486,490,498,501,505,614,655,679,681,764,796,954,969
	45	EG.5.1	44	19,24,25,26,27,52,83,142,144,146,183,213,252,339,346,368,371,373,375,376,405,408,417,440,445,446,456,460,477,478,484,486,490,498,501,505,614,655,679,681,764,796,954,969
	46	DV.7.1	45	19,24,25,26,27,142,147,152,157,185,210,213,257,339,346,371,373,375,376,405,408,417,440,444,446,452,455,456,460,477,478,484,486,498,501,505,614,655,679,681,764,796,858,954,969
P-lineage	47	JN.1	60	19,21,24,25,26,27,50,69,70,127,142,144,157,158,211,212,213,216,245,264,332,339,356,371,373,375,376,403,405,408,417,440,445,446,450,452,455,460,477,478,481,483,484,486,498,501,505,554,570,614,621,655,679,681,764,796,939,954,969,1143
	48	BA.2.86.1	59	19,21,24,25,26,27,50,69,70,127,142,144,157,158,211,212,213,216,245,264,332,339,356,371,373,375,376,403,405,408,417,440,445,446,450,452,460,477,478,481,483,484,486,498,501,505,554,570,614,621,655,679,681,764,796,939,954,969,1143
	49	BA.2.86	58	19,21,24,25,26,27,50,69,70,127,142,144,157,158,211,212,213,216,245,264,332,339,356,371,373,375,376,403,405,408,417,440,445,446,450,452,460,477,478,481,484,486,498,501,505,554,570,614,621,655,679,681,764,796,939,954,969,1143
	50	JN.2	59	19,21,24,25,26,27,50,69,70,127,142,144,157,158,211,212,213,216,245,264,332,339,356,371,373,375,376,403,405,408,417,440,445,446,450,452,460,477,478,481,483,484,486,498,501,505,554,570,614,621,655,679,681,764,796,939,954,969,1143

			1,505,554,570,614,621,655,679,681,764,796,939,954,969,1143
51	JN.1.7	62	19,21,24,25,26,27,50,69,70,127,142,144,157,158,211,212,213,216,245,264,332,339,356,371,373,375,376,403,405,408,417,440,445,446,450,452,455,460,477,478,481,483,484,486,498,501,505,554,570,572,614,621,655,679,681,764,796,939,954,969,1143,1150
52	JN.1.18	57	19,21,50,69,70,127,142,144,157,158,211,212,213,216,245,264,332,339,346,356,371,373,375,376,403,405,408,417,440,445,446,450,452,455,460,477,478,481,483,484,486,498,501,505,554,570,614,621,655,679,681,764,796,939,954,969,1143
53	JN.1.11.1	62	19,21,24,25,26,27,50,69,70,127,142,144,157,158,211,212,213,216,245,264,332,339,356,371,373,375,376,403,405,408,417,440,445,446,450,452,455,456,460,477,478,481,483,484,486,498,501,505,554,570,614,621,655,679,681,764,796,939,954,969,1104,1143
54	KP.3.1.1	64	19,21,24,25,26,27,31,50,69,70,127,142,144,157,158,211,212,213,216,245,264,332,339,356,371,373,375,376,403,405,408,417,440,445,446,450,452,455,456,460,477,478,481,483,484,486,493,498,501,505,554,570,614,621,655,679,681,764,796,939,954,969,1104,1143
55	KP.2	59	19,21,50,69,70,127,142,144,157,158,211,212,213,216,245,264,332,339,346,356,371,373,375,376,403,405,408,417,440,445,446,450,452,455,456,460,477,478,481,483,484,486,498,501,505,554,570,614,621,655,679,681,764,796,939,954,969,1104,1143
56	JN.1.37	61	19,21,24,25,26,27,50,69,70,127,142,144,157,158,211,212,213,216,245,264,332,339,356,371,373,375,376,403,405,408,417,440,445,446,450,452,455,460,477,478,481,483,484,486,498,501,505,554,570,614,621,655,679,680,681,764,796,939,954,969,1143
57	XEB	61	19,21,24,25,26,27,50,69,70,127,142,144,157,158,211,212,213,216,245,264,332,339,356,371,373,375,376,403,405,408,417,440,445,446,450,452,455,460,477,478,481,483,484,486,498,501,505,554,570,614,621,655,679,681,764,796,939,954,969,1143,1174
58	XDQ.1	55	19,21,24,25,26,27,50,69,70,127,142,144,157,158,211,212,213,216,245,264,332,339,356,371,373,375,376,403,405,408,417,440,445,446,450,452,460,475,483,484,486,498,501,505,554,570,614,621,655,679,681,764,796,954,969
59	KP.3	63	19,21,24,25,26,27,50,69,70,127,142,144,157,158,211,212,213,216,245,264,332,339,356,371,373,375,376,403,405,408,417,440,445,446,450,452,455,456,460,477,478,481,483,484,486,493,498,501,505,554,570,614,621,655,679,681,764,796,939,954,969,1104,1143
60	LB.1	64	19,21,24,25,26,27,31,50,69,70,127,142,144,157,158,183,211,212,213,216,245,264,332,339,346,356,371,373,375,376,403,405,408,417,440,445,446,450,452,455,456,460,477,478,481,483,484,486,498,501,505,554,570,614,621,655,679,681,764,796,939,954,969,1143
61	KP.1	63	19,21,24,25,26,27,50,69,70,127,142,144,157,158,211,212,213,216,245,264,332,339,356,371,373,375,376,403,405,408,417,440,445,446,450,452,455,456,460,477,478,481,483,484,486,498,501,505,554,570,614,621,655,679,681,764,796,939,954,969,1086,1104,1143
62	KS.1	58	50,59,69,70,127,142,144,157,158,211,212,213,216,245,264,332,339,346,356,371,373,375,376,403,405,408,417,440,445,464,450,452,455,456,460,477,478,481,483,484,486,498,501,505,554,570,614,621,655,679,681,764,796,939,954,969,1087,1143
63	KP.1.1.3	65	19,21,24,25,26,27,31,50,69,70,127,142,144,157,158,211,212,213,216,245,264,332,339,346,356,371,373,375,376,403,405,408,417,440,445,446,450,452,455,456,460,477,478,481,483,484,486,498,501,505,554,570,614,621,655,679,681,764,796,939,954,969,1086,1104,1143
64	XDV.1	56	19,21,50,69,70,127,142,144,157,158,211,212,213,216,245,264

			4,332,339,356,371,373,375,376,403,405,408,417,440,445,446,450,452,455,456,460,477,478,481,484,486,498,501,505,554,570,614,621,655,679,681,764,796,939,954,969,1143
65	LP.1	66	19,21,24,25,26,27,31,50,69,70,127,142,144,157,158,211,212,213,216,245,264, 332,339,346,356,371,373,375,376,403,405,408,417,440,445,446,450,452,455,456,460,477,478,481,483,484,486,498,501,505 ,554,570,614,621,655,679,681,764,796,939,954,969,1086,1104,1143,1229
66	XED	64	19,21,24,25,26,27,31,50,69,70,127,142,144,157,158,211,212,213,216,245,264, 332,339,346,356,371,373,375,376,403,405,408,417,440,445,446,450,452,455,456,460,477,478,481,483,484,486,498,501,505 ,554,570,614,621,655,679,681,764,796,939,954,969,1143,1263
67	XEC	65	19,21,22,24,25,26,27,50,59,69,70,127,142,144,157,158,211,212,213,216,245,264, 332,339,356,371,373,375,376,403,405,408,417,440,445,446,450,452,455,456,460,477,478,481,483,484,486,493,498,501,505 ,554,570,614,621,655,679,681,764,796,939,954,969,1104,1143
68	LF.7	67	19,21,22,24,25,26,27,31,50,69,70,127,142,144,157,158,182,190,211,212,213,216,245,264, 332,339,346,356,371,373,375,376,403,405,408,417,440,444,445,446,450,452,455,456,460,477,478,481,483,484,486,498,501,505 ,554,570,614,621,655,679,681,764,796,939,954,969,1143
69	LF.7.1.2	68	19,21,22,24,25,26,27,31,50,69,70,127,142,144,157,158,182,190,211,212,213,216,245,264, 332,339,346,356,371,373,375,376,403,405,408,417,440,444,445,446,450,452,455,456,460,475,477,478,481,483,484,486,498,501,505 ,554,570,614,621,655,679,681,764,796,939,954,969,1143
70	LP.8.1	68	19,21,24,25,26,27,31,50,69,70,127,142,144,157,158,186,190,211,212,213,216,245,264, 332,339,346,356,371,373,375,376,403,405,408,417,440,445,446,450,452,455,456,460,477,478,481,483,484,486,493,498,501,505 ,554,570,614,621,655,679,681,764,796,939,954,969,1086,1104,1143
total		153	3,5,9,12,13,18,19,20,21,22,24,25,26,27,31,50,52,59,67,69,70,75,76,80,83,95,127,136,138,142,143,144,145,146,147,152,156,157,158,180,182,183,185,186,190,209,210,211,212,213,215,216,222,241,242,243,244,245,246,247,248,249,250,251,252,253,257,264, 332,339,346,356,357,368,371,373,375,376,403,405,408,417,439,440,444,445,446,449,450,452,455,456,460,475,477,478,481,483,484,486,490,493,496,498,501,505 ,547,554,570,572,613,614,621,655,677,679,680,681,701,703,704,716,764,769,796,856,858,859,888,899,939,950,954,969,981,982,1020,1027,1071,1086,1087,1092,1101,1104,1118,1130,1139,1143,1150,1174,1176,1229,1263

NMS: number of mutated sites; Mutated sites are considered when they occur in at least 75% of the SARS-CoV-2 lineage sequences. Mutations in the spike protein's receptor-binding domain (RBD) are indicated in bold.

Note: 70 variants written in red are taken from the mutation reports provided by non- VOC samples in outbreak.info. It leads to the total number of mutated sites from 147 (in original case of 63 variants) increased to 153.

Table S4 New variants of SARS-CoV-2

A total of 9 variants from the mutation reports provided by NextStrain

(https://nextstrain.org/ncov/gisaid/global/6m, accessed on 7 September 2025)

variant	NMS	Collection date	mutated sites
XEC.25.1	66	2025/3/3	19,21,22,24,25,26,27,50,59,69,70,127,144,142,157,158,211,212,213,216,245,264, 332,339,356,371,373,375,376,403,405,408,417,435,440,445,446,450,452,455,456,460,477,478,481,483,484,486,493,498,501,505 ,554,570,614,621,655,679,681,764,796,939,954,969,1104,1143
NB.1.8.1	66	2025/3/15	19,21,22,24,25,26,27,50,59,69,70,127,142,144,157,158,184,211,212,213,216,245,264, 332,339,356,371,373,375,376,403,405,408,417,435,440,445,446,450,452,455,456,460,477,478,481,483,484,486,493,498,501,505 ,554,570,614,621,655,679,681,764,796,939,954,969,1143
XFH.2	67	2025/4/30	19,21,22,24,25,26,27,31,50,69,70,127,142,144,157,158,182,190,213,216,245,264, 332,335,339,346,356,371,373,375,376,385,403,405,408,417,440,445,446,450,452,455,456,460,477,478,481,484,486,493,498,501,505 ,554,570,614,621,655,677,679,681,764,796,939,954,969,1143
LP.8.1.1	69	2025/4/26	5,19,21,24,25,26,27,31,50,69,70,127,142,144,157,158,186,190,211,212,213,216,245,264, 332,339,346,356,371,373,375,376,403,405,408,417,440,445,446,450,452,455,456,460,477,478,481,483,484,486,493,498,501,505 ,554,570,614,621,655,679,681,764,796,939,954,969,1086,1104,1143
LF.7.9	69	2025/5/13	19,21,22,24,25,26,27,31,50,69,70,127,142,144,157,158,182,190,211,212,213,216,245,264, 332,339,346,356,371,373,375,376,403,405,408,417,440,441,444,445,446,450,452,455,456,460,475,477,478,481,483,484,486,498,501,505 ,554,570,614,621,655,679,681,764,796,939,954,969,1143
XFG	70	2025/3/20	19,21,22,24,25,26,27,31,50,69,70,127,142,144,157,158,182,190,211,212,213,216,245,264, 332,339,346,356,371,373,375,376,403,405,408,417,440,444,445,446,450,452,455,456,460,477,478,481,483,484,486,487,493,498,501,505 ,554,570,572,614,621,655,679,681,764,796,939,954,969,1143
XFV	71	2025/6/12	19,21,22,24,25,26,27,31,50,69,70,127,142,144,157,158,182,190,211,212,213,216,245,264, 332,339,346,356,371,373,375,376,403,405,408,417,440,444,445,446,450,452,455,456,460,477,478,481,483,484,486,487,493,498,501,505 ,554,570,572,614,621,655,679,680,681,764,796,939,954,969,1143
LF.7.9.1	72	2025/2/6	17,18,19,20,21,22,23,24,25,26,27,31,50,69,70,127,142,144,157,158,182,190,211,212,213,216,245,264, 332,339,346,356,371,373,375,376,403,405,408,440,441,444,445,446,450,452,455,456,460,475,477,478,481,483,484,486,498,501,505 ,554,570,614,621,655,679,681,764,796,939,954,969,1143
BA.3.2.2	74	2025/4/4	9,21,26,67,69,70,95,101,136,137,138,139,140,141,142,143,144,145,146,147,157,164,172,187,211,212,242,243,251,326, 339,348,356,371,373,375,403,405,408,417,435,440,445,446,452,460,477,478,484,496,498,501,529 ,554,575,583,614,625,641,642,654,655,679,681,688,704,764,795,796,852,939,954,969,1184

Table S5 Retrieval of SARS-CoV-2 variant data in Table S3: The number of mutated sites (NMS) in the spike protein and the first global sample collection dates for each variant arranged in chronological order

Macro-lineage	Variant	NMS *	Earliest date ‡	Variant	NMS *	Earliest date ‡
N-lineage	B.1	1	15 Jan 2020	B.1.621	9	19 Sep 2020
	B.1.177	2	7 Mar 2020	R.1	4	24 Oct 2020
	B.1.1.176	3	12 Mar 2020	C.37	14	8 Nov 2020
	D.2	2	19 Mar 2020	B.1.526	4	15 Nov 2020
	P.2	3	15 Apr 2020	B.1.525	9	11 Dec 2020
	B.1.1.7	10	14 May 2020	C.36.3	9	4 Jan 2021
	B.1.429	4	6 Jul 2020	P.3	7	15 Jan 2021
	B.1.351	10	9 Jul 2020	AZ.2	6	5 Feb 2021
	B.1.617.2	9	7 Sep 2020	AV.1	10	23 Mar 2021
	P.1	12	11 Sep 2020	B.1.1.529	7	15 Apr 2021
	B.1.617.1	5	15 Sep 2020	C.1.2	15	11 May 2021
O-lineage	BA.1	33	27 Jan 2021	BN.1.2	40	7 Feb 2022
	BA.1.1	35	28 Jan 2021	CH.1.1	41	12 May 2022
	BA.2	31	25 Mar 2021	XBB.1.5	42	12 Jun 2022
	BA.2.12.1	33	28 Sep 2021	BM.4.1.1	39	20 Jul 2022
	BA.2.65	31	11 Oct 2021	XBC.1	39	6 Sep 2022
	BA.1.1.15	37	27 Nov 2021	CH.1.1.1	42	15 Oct 2022
	BA.5	34	9 Dec 2021	XBB.1.16	43	4 Jan 2023
	BA.4.1	35	14 Dec 2021	EG.1	43	16 Jan 2023
	BQ.1.1	37	20 Dec 2021	HV.1	46	29 Jan 2023
	BA.2.75	30	31 Dec 2021	HK.3	45	29 Jan 2023
	BF.5	35	8 Jan 2022	EG.5.1	44	31 Jan 2023
	BF.7	35	24 Jan 2022	DV.7.1	45	29 May 2023
P-lineage	JN.1	60	13 Jan 2023	KP.3	63	7 Jan 2024
	BA.2.86.1	59	17 Jan 2023	LB.1	64	15 Jan 2024
	BA.2.86	58	11 Mar 2023	KP.1	63	1 Feb 2024
	JN.2	59	22 Jun 2023	KS.1	58	15 Feb 2024
	JN.1.7	62	25 Sep 2023	KP.1.1.3	65	23 Feb 2024
	JN.1.18	57	11 Dec 2023	XDV.1	56	26 Feb 2024
	JN.1.11.1	62	29 Dec 2023	LP.1	66	22 Apr 2024
	KP.3.1.1	64	1 Jan 2024	XED	64	19 Jun 2024
	KP.2	59	2 Jan 2024	XEC	65	28 Jun 2024
	JN.1.37	61	3 Jan 2024	LF.7	67	26 Aug 2024
	XEB	61	3 Jan 2024	LF.7.1.2	68	8 Sep 2024
	XDQ.1	55	5 Jan 2024	LP.8.1	68	19 Sep 2024

* NMS: number of mutated sites. ‡ Dates : the worldwide first sample collection date.

Supplementary Material 2: Phylogenetic tree obtained by cladogenesis algorithm

Figure S1 Phylogenetic tree of 25 mutants (total number of mutated sites =104) in 4-letter representation

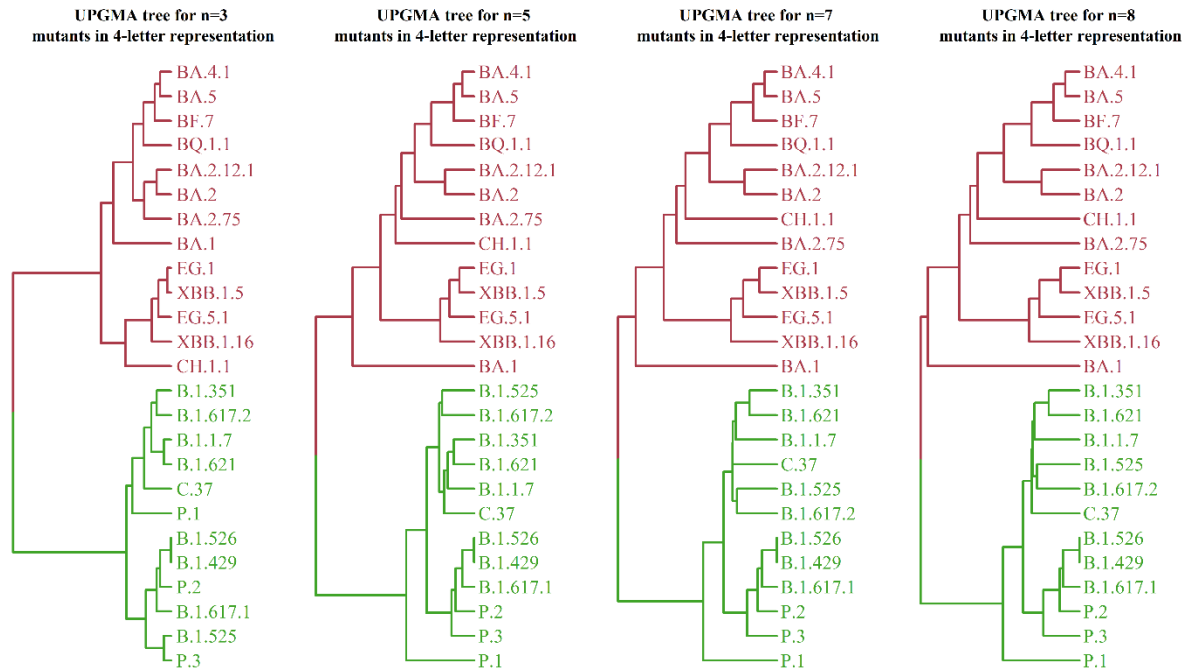
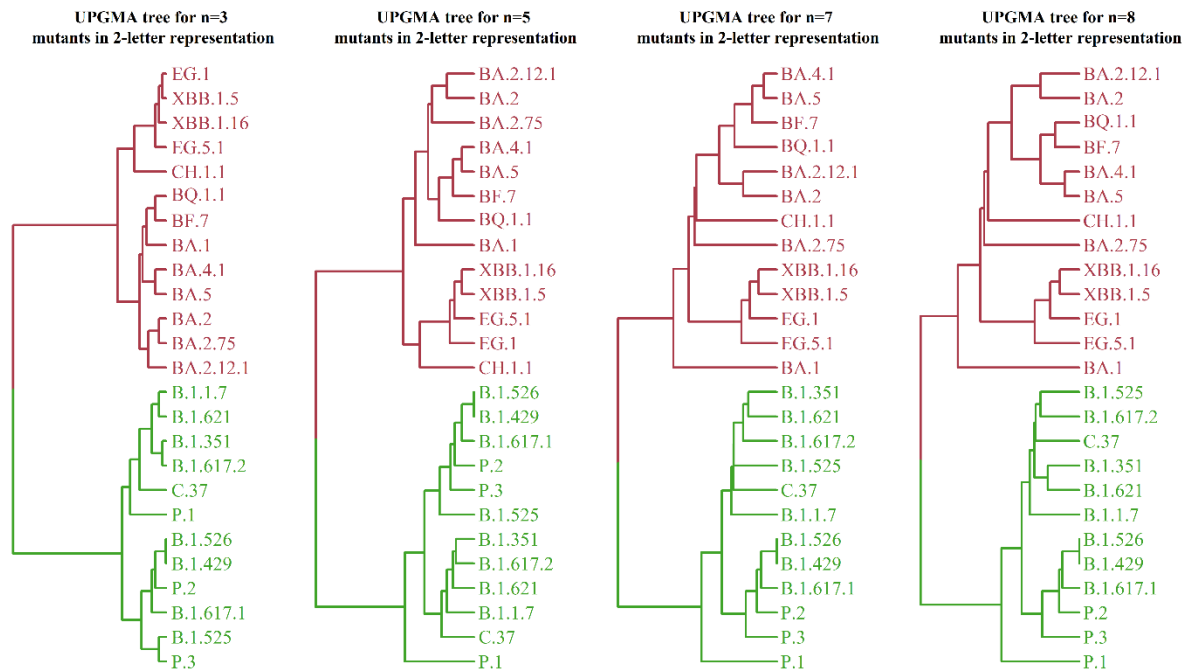


Figure S2 Phylogenetic tree of 25 mutants (total number of mutated sites =104) in 2-letter representation



Figures S1 and S2 above show the comparison of cladogram structures of phylogenetic trees with different n values and letter representations.